Heliyon 10 (2024) e23936

Contents lists available at ScienceDirect

Heliyon

journal homepage: www.cell.com/heliyon

Research on the application of inertially stabilized platform in the dynamic measurement of cold atomic gravimeter

Pei-jun Chen [a,b,1], Min-rui Jiang [a,1], Xiao-feng Lv [a], Hang Zhou [a], Di Yang [a], Ying Zhou [a], Zifan Jin [a], Shu-ping Peng [a,*]

[a] Zhejiang Provincial Key Laboratory of Quantum Precision Measurement, College of Science, Zhejiang University of Technology, Hangzhou 310023, China

[b] School of mechanical and electrical engineering, Huangshan College, Huangshan 245041, China

ARTICLE INFO

Keywords:
Inertially stabilized platform
High precision horizontal attitude
Cold atomic gravimeter
Absolute gravity measurement

ABSTRACT

Dynamic gravity field measurement based on the cold atom absolute gravity measurement system has important applications in geological exploration, gravity field mapping and other fields. The inertial stabilized platform is the key component of the dynamic cold atom absolute gravity measurement system, which can isolate the interference of carrier angle motion and keep the atomic gravimeter probe in the horizontal attitude during the measurement process. In this paper, according to the dynamic measurement requirements of atomic gravimeter, a high-precision two-axis inertial stabilized platform system is designed. The relationship between attitude angle and gravity measurement error is analyzed, and the stability of the system is enhanced by lead-lag method. Then the static vertical vibration power spectrum of the platform is measured to consider its influence on dynamic gravity measurement. Finally, a dynamic gravity test experiment was conducted in the Yellow Sea to verify the attitude control accuracy of the platform, and the attitude data of the platform under different heading were evaluated. The attitude standard deviation of the platform was better than 4×10^{-5} rad, and the absolute gravity standard deviation of the linear round-trip measurement reached 1.49 mGal. The experimental data show that the inertial stabilized platform can meet the dynamic measurement requirements of the cold atom gravimeter.

1. Introduction

At present, high precision ground gravity observation information, which can obtained from the gravimeter, is the basic data for studying the characteristics of the earth's internal structure, density and stress distribution [1,2]. The instruments used for gravity measurement are divided into two categories, relative gravimeters and absolute gravimeters [3]. The working principle and application of the two are different. The absolute gravimeter can directly measure the value of the acceleration of gravity where it is, which is the reference information of gravity, and then the relative gravimeter can be measured around, it can not directly measure the acceleration of gravity, it can only measure the difference between two points. However, the relative gravimeter often needs to be calibrated at the reference point because of the problems such as instrument drift, spring response and calibration factor change [4,5].

* Corresponding author.
E-mail address: pengshuping@zjut.edu.cn (S.-p. Peng).
[1] These authors contributed equally to this work.

https://doi.org/10.1016/j.heliyon.2023.e23936
Received 4 June 2023; Received in revised form 4 December 2023; Accepted 15 December 2023
Available online 17 December 2023

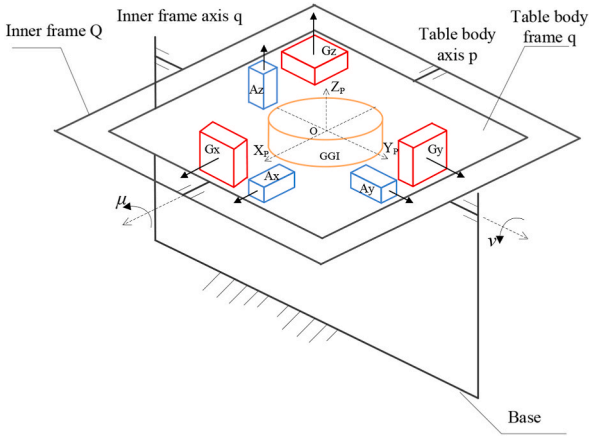

Fig. 1. Schematic diagram of two-axis platform's principle.

Absolute gravimeters have been developed in the last thirty years, it is mainly divided into two categories, optical absolute gravimeter [6] and cold atom absolute gravimeter [7]. The optical absolute gravimeter uses laser to measure the falling distance of the slider in the vacuum channel and then calculates the gravitational acceleration. The rapid development of atomic interferometer has been driven by laser-cooled atomic technology and matter-wave interference methods [8,9]. Nowadays, the measurement accuracy of cold atomic gravimeter(CAG) is the same as the optical absolute gravimeters [10]. Compared with the these, the volume of cold atom is very small, and the miniaturized vacuum measuring device is easy to achieve, while the mechanical transmission device of optical gravimeter is complex, which is not conducive to the development of dynamic absolute gravity measurement. The miniaturized and movable CAG has been taken out of the laboratory [11–13] and gradually applied in geophysics, space exploration, resource exploration and marine physical field mapping due to the integration of embedded control technology into the atomic gravimeter [14–16].

Since the acceleration of gravity itself is vertical downward, for both the absolute gravimeter and the relative gravimeter, it is necessary to maintain a horizontal attitude when measuring gravity, which can reduce the measurement error [17–19]. The researchers have carried out the relative gravity measurement combined the inertially stabilized platform and the relative gravimeter [20–22], such as the CHZ-II relative gravimeter combined with a strapdown stabilized platform to form a dynamic measurement system, the control accuracy of the platform is greater than 1.45×10^{-4} rad, but the device was unable to complete the long-distance and long-term gravity measurement tasks. Based on the advantages of absolute gravity measurement, dynamic absolute gravity measurement experiments on ship, vehicle and airborne have been carried out. The team of Bidel.Y has conduct several dynamic comparative experiments between the CAG and the relative gravimeter on shipborne and airborne from 2016 to 2022 [23–25]. In these experiments, the CAG has been fixed in a two-axis Inertially Stabilized Platform(ISP) in order to ensure that the axis of Raman optical coincides with the gravitational acceleration perpendicular, the result show a good agreement for the cold atom gravimeter with standard deviation and means on difference below or equal to 2 mGal, the attitude control accuracy of the platform is 0.1×10^{-3} rad. The team of Che also carried out a test using a CAG and a ISP on Qiandao Lake in 2022, the control accuracy of the roll is 0.08×10^{-3} rad, and the pitch is 0.03×10^{-3} rad [26].

Our team carried out a vehicle-mounted fixed-point absolute gravity experiment on the roadside of Xianlin Reservoir in Hangzhou, we used a three-axis leveling platform to control the tilt angle which is unsuitable for dynamic measurement [27]. Therefore, we have developed a set of ISP in order to further develop the dynamic experiment of CAG. Then, our team has formed a dynamic absolute gravity measurement system combining an ISP and a CAG, and gradually carried out moving experiments [28], mooring experiments [29], lake and ocean comparison experiments [30].

Inertially stabilized platform [31–33] are widely used in image tracking [34,35], attitude control [36,37] and so on. The main function of the ISP is to restrain the interference torque and isolate the carrier movement to ensure that the frame is always in the geographical horizontal plane. The structure of the platform is composed of the frame, motor, sensor and controller, and the system is divided into the correction loop and the stabilization loop. The correction loop can calculate the angle and angle velocity of the platform based on information from the accelerometer and gyro; the stabilization loop is used to restrain the interference torque and keep the platform attitude stable.

The CAG is larger and heavier than relative gravimeters. The vacuum probe for cold atom interferometry used in this paper is a cylinder with a diameter of 520 mm and a weight of 60 kg. To ensure the rigidity of the platform, the thickness of the platform frame and the rotational inertia must be excessive. Based on the practical needs of dynamic absolute gravimetry, this paper designs a highly precision ISP, analyzes how much the control accuracy of the platform that can meet the measurement requirements, introduces the frame structure and control system structure of the platform, assesses the impact of the platform on the sensitivity of the CAG, and analyzing the attitude data of the ISP from dynamic absolute gravimetry field experiments on the Yellow Sea.

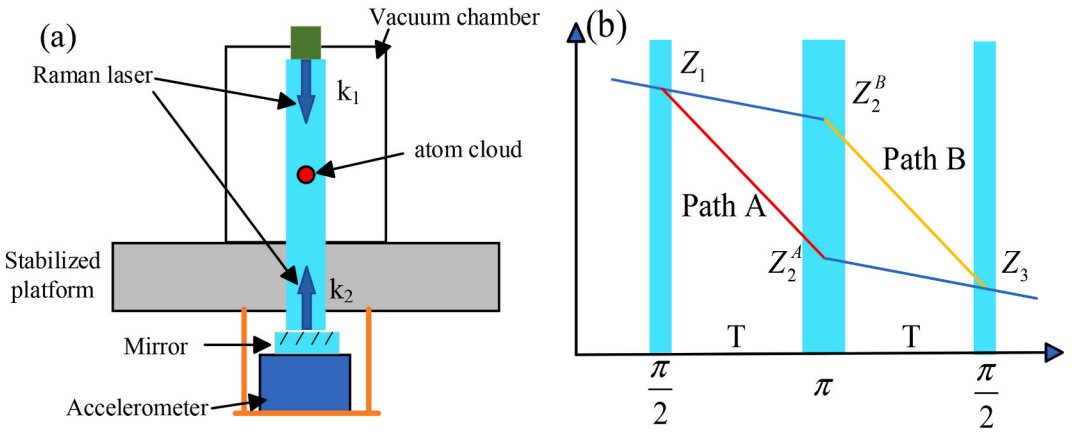

(a) Schematic diagram of working principle (b) The diagram of atomic interference path

Fig. 2. The schematic diagram of absolute gravity measurement system.

2. Principle and structure

2.1. The principle of ISP

The two-axis stabilized platform actually causes the platform coordinate system (p coordinate system) to track the horizontal attitude angle of the geographic coordinate system (n coordinate system), so there is only the azimuth angle H between the p coordinate system and the n coordinate system, maintaining the geographic horizontal attitude, as shown in Fig. 1.

Take the frame axis q as an example, when the carrier has an angular velocity v around the frame axis q direction, the corresponding Gy gyroscope is sensitive to the angular velocity information and sends the angular velocity increment to the stabilization control loop, which generates a torque signal of equal magnitude and opposite direction to the angular velocity to control the rotation of the torque motor of the axis, so as to keep the axis stable and isolate the influence of disturbance.

2.2. The attitude index of ISP

The CAG developed by our team is based on a Mach-Zehnder atomic interferometer [15]. The basic principle is that the cold atom cloud falls freely in the vacuum probe, and it splits, deflects and combines by three pulses of reversed Raman light, and finally realizes the interference of atomic matter waves, as shown in Fig. 2(a)(b).

The atom cloud after split by the Raman lights goes through two paths A and B respectively, and the total phase of the atomic interference is related to the trajectory of the two paths and the phase sum of the two beams of Raman light, the expression is shown in Formula (1),

$$\Delta\varphi = \varphi_A - \varphi_B = \varphi(z_1) - \varphi\left(z_2^A\right) - \varphi\left(z_2^B\right) + \varphi(z_3) \tag{1}$$

z_1, z_A 2, z_B 2, z_3 is the position of the atom in the light field, Φ is the phase of light. The main gravity error of the measurement comes from changing of the total phase during the interference process, furthermore, the main reason of changing of the total phase is the vibration or rotation of the mirror which cause a change in phase of the reflected Raman light. From Fig. 2(a), the mirror is fixed on the accelerometer and also on the ISP frame, then the attitude change of the platform leads to the vibration and rotation of the mirror, so a change in the total phase is caused finally. Under the static conditions, the simple formula for calculating the tilt of an axis and gravity error is shown in Formula (2) [19],

$$\Delta g = \theta^2 \cdot g/2 \tag{2}$$

in the formula: Δg is the measurement error, g is the acceleration of gravity and θ is the tilt angle. The way to decrease measurement error is to reduce the value of the attitude tilt, for example, if we want to keep it within 1 mGal, we can calculate the corresponding θ to be 1.4×10^{-3} rad. However, in the process of a dynamic measurement, due to the horizontal acceleration of the carrier and the tilt of the platform, there is relative motion between the cold atom cloud and the Raman light. So, at the same value of tilt, the gravity error which is show in Formula (3) [24] must be greater than the calculation result of Formula (2),

$$\Delta g = \frac{\theta_x^2 + \theta_y^2}{2} \cdot g + \theta_x \cdot a_x + \theta_y \cdot a_y \tag{3}$$

in the formula: a_x, a_y is the horizontal acceleration. If assumed that the horizontal acceleration is 0.01 m/s^2, we also want to keep it within 1 mGal, then the value of θ_x *and* θ_y should be less than 0.5×10^{-3} rad. By the way, the process of atomic interference does not

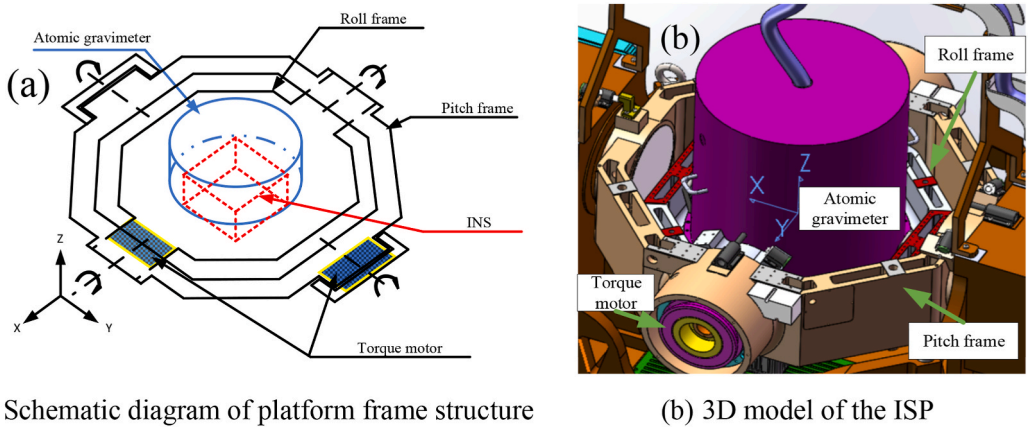

Fig. 3. Structure diagram of inertially stabilized platform.

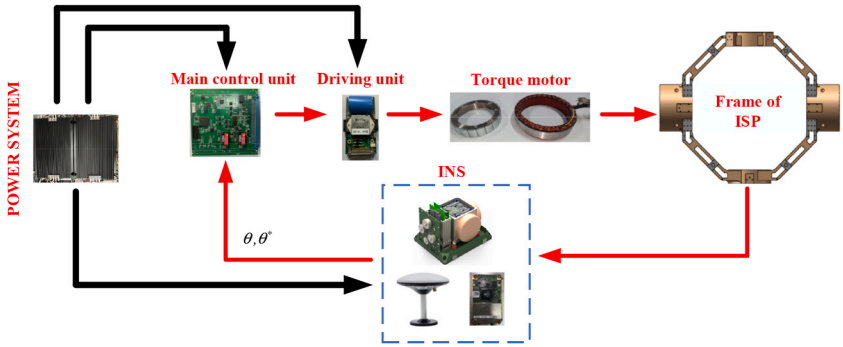

Fig. 4. The schematic of platform attitude control system.

require the azimuth of the carrier, and the gravitational error caused by the rotation of the Earth can be calculated by the Coriolis effect.

In summary, in dynamic measurement environment for CAG, the carrier is subjected to random external disturbance torque and horizontal acceleration, according to the working principle of the atomic gravimeter, we need a two-axis ISP to isolate the disturbance and keep the tilt value small, so that higher accuracy can be obtained.

2.3. *The structure of ISP*

The structure of the platform is shown in Fig. 3(a)(b). As can be seen from Fig. 3(a), the ISP consists of an inertial navigation system (INS), a frame (roll and pitch) and motors. The two axis are vertically mounted and fixed at both ends, the cross section of the two frames is hollow hexagonal structure, with the characteristics of large moment of inertia and strong stiffness, and the material is cast aluminum alloy. The 3D model effect is shown in Fig. 3(b), so that the structure of the platform can be intuitively understood. The atomic gravimeter is fixed on the roll frame, the outside of the roll frame is the pitch frame, and the DC motor marked in the figure is fixed on the roll frame, however the pitch frame motor is not marked in Fig. 3(b) due to line of sight obstruction.

The cylinder is the vacuum probe of the cold atom gravimeter, which is installed in the center of the platform table.The INS is mounted below the vacuum probe and is used to calculate the relevant information of the platform frame in inertial space, including the local geo-level and the carrier of the acceleration, angle, and angular velocity. The measurement accuracy of INS determines the attitude control effect. The high precision F120HC interferometric fiber optic gyro is selected as the angular velocity sensor of INS, constant drift is $\leq 0.003°/h$, which produces a horizontal attitude error of 2.5×10^{-5} rad in undamped state. The quartz flexible accelerometer was selected as the accelerometer sensor of INS, zero bias is ≤ 0.02 mg, it also produces a horizontal attitude error of 2.0×10^{-5} rad in undamped state. In combination with GPS antenna and receiver, INS estimates and compensates the measurement error through Kalman filter to improve the navigation accuracy.

The control system of the ISP is mainly composed of power supply system, main control unit, drive unit, torque motor, frame and INS, as shown in Fig. 4. The main components of the main control unit include microcontroller chip STM32F429 of *ST* Company. The main control unit outputs analog signals to the drive unit, and the drive unit uses PWM amplifier to generate DC linear voltage to control the torque motor rotation. The DC torque motor in the frame can control the rotation of frame at a very low speed, and the

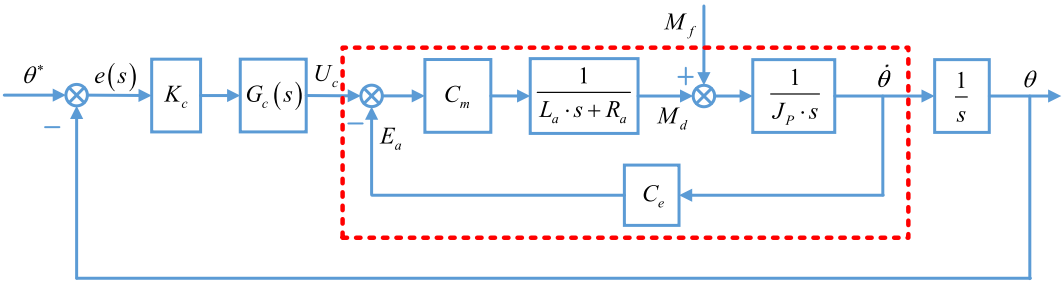

Fig. 5. The equivalent control diagram of DC torque motor.

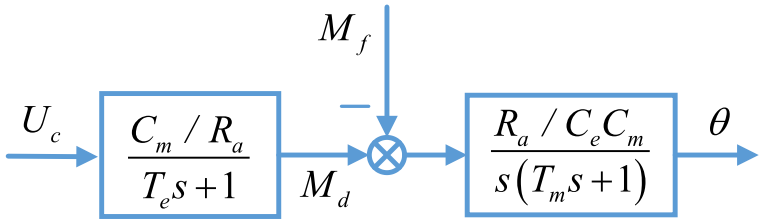

(a) The diagram of simplified open-loop equivalent of DC torque motor

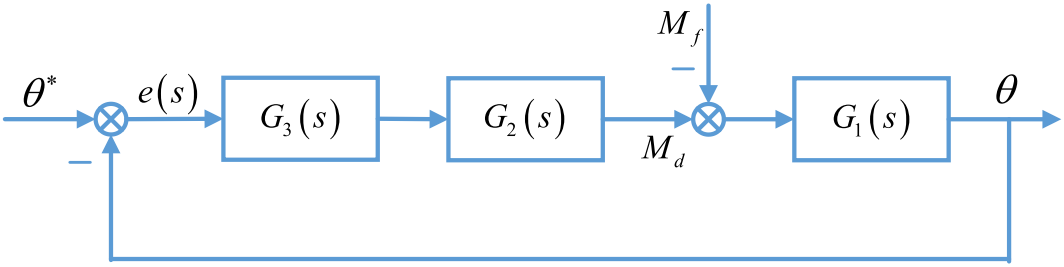

(b) The diagram of equivalent motor control based on unit negative feedback

Fig. 6. The equivalent control diagram of DC torque motor.

motor is in a blocked state, so the locked-torque of motor is greater than the moment of inertia of the frame. The models of two motors are 180LYX50 and 250LYX45, the corresponding peak locked-rotor moment is 25 N m and 65 N m. The motor shape is hollow structure, easy to thread and install.

3. Control parameter design and simulation

3.1. Parameter design

In order to realize the high precision attitude angle, the relevant parameters in the controller are designed and simulated. The block diagram of the torque motor control principle is shown in Fig. 5. In the figure, the equivalent control model of the DC motor is in the dotted box, C_m is the torque coefficient of the torque motor, C_e is the back-electromotive force coefficient of the torque motor, E_a is the back-electromotive force of armature, L_a is the armature inductance of armature, R_a is the armature resistance of armature, J_p is the total moment of inertia of the frame and the probe of gravimeter, M_d is the output torque of the torque motor, M_f is the disturbance torque on the frame, θ is the attitude angle of the frame, ω is the angular velocity of the frame. K_c is the open-loop gain, U_c is voltage output of the controller, $G_c(s)$ is the controller transfer function, θ^* is the local geographic horizontal attitude angle from INS.

Firstly, we simplify the motor model. Assuming the external interference is 0, the transfer function between the output of the motor and the control voltage is Formula (4),

* Funded by the National Natural Science Foundation of China (Grant No. 51905482).

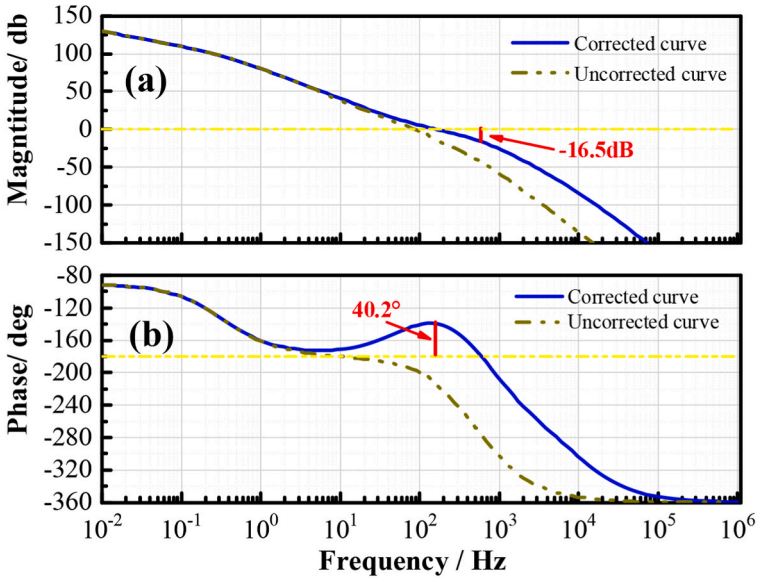

(a) The diagram of open-loop amplitude-frequency characteristic

(b) The diagram of open-loop phase-frequency characteristic

Fig. 7. Comparison chart of open-loop frequency response curve of rolling frame system between before and after correction.

$$\frac{\theta(s)}{U_c(s)} = \frac{1/C_e}{s(T_m s+1)(T_e s+1)} \tag{4}$$

where, T_m is electrical time constant,T_e is mechanical time constant. Then, assuming the control voltage is 0, the transfer function between the output of the motor and the interference torque is Formula (5),

$$\frac{\theta(s)}{M_f(s)} = -\frac{R_a}{C_e C_m s(T_m s+1)} \tag{5}$$

The simplified motor model is open-loop structure, which is shown as in Fig. 6(a). The control system is organized into a unit negative-feedback structure, which is shown as in Fig. 6(b), which combines the open-loop gain and the corrector transfer function.

The three transfer functions in the forward channel are shown in Formula (6)(7)(8),

$$G_1(s) = \frac{R_a/C_e C_m}{s(T_m s+1)} \tag{6}$$

$$G_2(s) = \frac{C_m/R_a}{(T_e s+1)} \tag{7}$$

$$G_3(s) = K_c G_c(s) \tag{8}$$

From Fig. 6(b), the input of the control system is the set angle and interference torque of the platform, the output is the actual angle of the platform. In order to effectively suppress the influence of interference torque and improve the accuracy of the following the set angle, we deduce closed-loop transfer functions of angle following and interference suppression respectively which is shown in Formula (9)(10),

$$\frac{\theta(s)}{\theta^r(s)} = \frac{G_1(s)G_2(s)G_3(s)}{1+G_1(s)G_2(s)G_3(s)} \tag{9}$$

$$\frac{\theta(s)}{M_f(s)} = \frac{-G_1(s)}{1+G_1(s)G_2(s)G_3(s)} \tag{10}$$

According to the final-value theorem in the principle of automatic control, the stiffness coefficient is defined as k_s which is Formula (11),

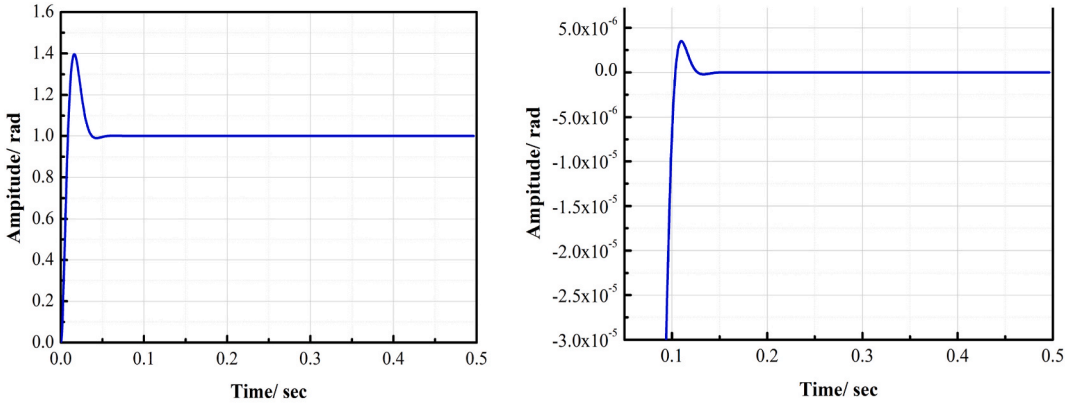

(a) Unit step response curve (b) The steady state error of unit step response curve

Fig. 8. The result of steady-state error simulation on unit step response.

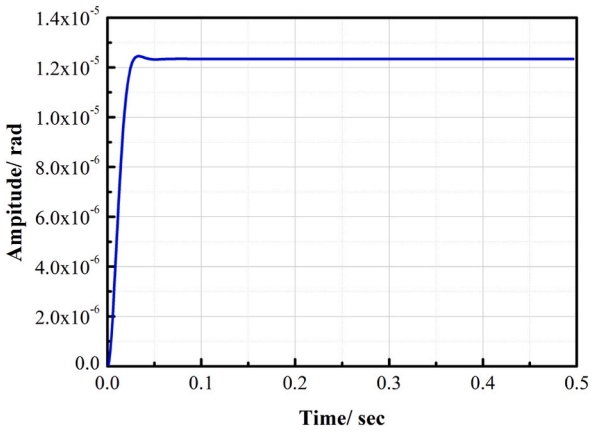

Fig. 9. Response curve of restraining disturbance torque of corrected system of rolling frame.

$$k_s = \lim_{s\to 0} \frac{M_f(s)}{\alpha(s)} = \frac{K_c \cdot C_m}{R_a} \tag{11}$$

Taking the roll frame as an example for analysis, according to the measurement requirements of the cold atomic gravimeter, the maximum disturbance torque is set at 3.92 N·m, and the angle variation range is at 4.85×10^{-5} rad, the value of k_s is 8.1×10^4 N m rad^{-1}, in addition, the C_m is 7.64 N m A^{-1} and R_a is 22.67Ω. Then the open-loop gain K_c is calculated to be 2.4503×10^5.

If the open-loop gain is used directly into the control system, the close-loop system is unstable. So we use traditional lead-lag correctors which is shown as Formula (12) to make the system stable.

$$G_c(s) = \frac{(a_1 s + 1)(a_2 s + 1)}{(b_1 s + 1)(b_2 s + 1)} \tag{12}$$

3.2. Control system simulation

The simulation is used to verify that the parameters of the corrector can meet the stability requirements of the system, such as the open-loop bode diagram, the steady-state error of angle following, and the dynamic response of disturbance torque.

Taking the roll frame as an example. The calibrator parameters were chosen as $a_1 = 0.0015$, $a_2 = 0$, $b_1 = 0.00009$, $b_2 = 0$, $L_a = 43.8$ mH, $C_e = 7.64$V·(rad/s)$^{-1}$ and $J_P = 7.5$ kg m^2. The amplitude-frequency and phase-frequency characteristics curves of the open-loop transfer function before and after correction is shown in Fig. 7(a)(b), the solid blue line is the curve after correction, and the dashed brown line is the curve before correction.

It can be seen that the system is unstable before correction, after correction the system has a phase angle margin of 40.2° in Fig. 7(b) and an amplitude margin of 16.5 dB in Figure(a), which meets the stability requirements.

Then we analyze the steady-state error of the system. The motor parameters, calibration parameters, open-loop gain are brought

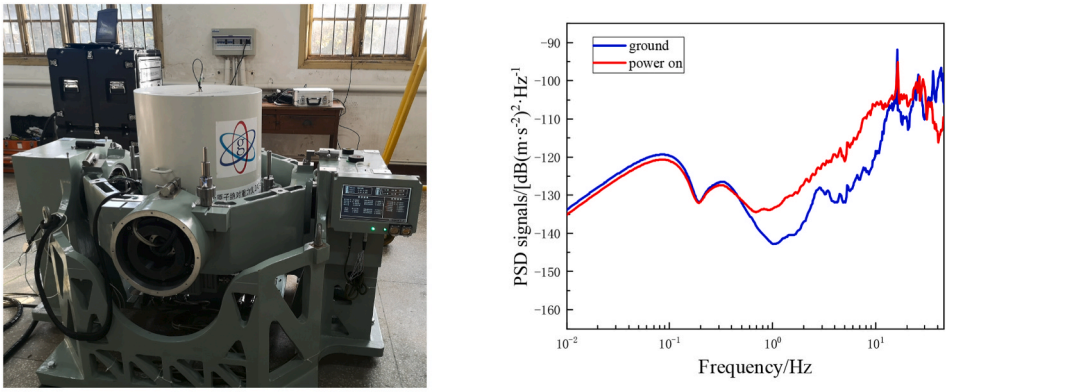

(a) The photo of static test (b) Comparison of vertical vibration power spectrum line

Fig. 10. Comparison experiment of vertical vibration test of platform.

into the close-loop transfer function such as Formula (9), the input is a unit step response, the response curve is shown in Fig. 8(a). It can be seen that the response curve has an overshoot of 40 % and a regulation time of 50 ms, the steady-state error curve is shown in Fig. 8(b).

Finally, we analyze the dynamic response of interference torque, the parameters are also brought into the close-loop transfer function such as Formula (10). The input is a step signal of 3.92 N m, the response curve is shown in Fig. 9, with a regulation time of 30 ms and an attitude change amplitude of 1.23×10^{-5} rad.

The simulation results show that the amount of overshoot is sacrificed to speed up the adjustment time, and the overshoot of the angle following is large. The stabilization loop is able to accurately follow the local geographical level solved by the correction loop, the curve of interference moment suppression is smooth, and the stabilization loop can effectively suppress the interference moment and keep the attitude stable to meet the measurement requirements of the atomic gravimeter.

4. Experiment

To investigate the working performance of the inertially stabilized platform, a set of dynamic absolute gravity measurement system was composed by the cold atomic gravimeter and the inertially stabilized platform, and the static vertical vibration performance of the platform was evaluated, and absolute gravity measurement experiments were carried out under ship mooring and under navigation in the Yellow Sea.

4.1. Vertical vibration test

When the platform is in operation, the stabilization loop generates a small angular acceleration during the adjustment process, the projection of which in the vertical direction is equivalent to a vertical vibration. Consequently, the effect of operating the inertially stabilized platform on vertical vibration is first assessed, as shown in Fig. 10(a). In the experiment, the vacuum probe was rigidly connected to the inertial stabilization platform and then rested on the laboratory floor with shock absorbers during the night (when there was little human activity).The test instrument uses a seismometer (Güralp 3ESPC) as a vibration sensor with an effective bandwidth of 0.017–100Hz, a sensitivity of approximately 2000 $Vm^{-1}s^{-1}$ and a noise floor below NLNM (New Low Noise Model) [38]. Fig. 9(b) shows the test results.

The blue curve in Fig. 10(b) shows the vibration power spectrum at ground level, which mainly reflects the environmental vibration information at the measurement site, and the red power spectrum is the power spectrum when the platform is operating, which includes the vertical vibration information when the motor is operating. From the figure it can be seen that the vibration noise generated by the operation of the platform is mainly concentrated in the range 0.5Hz–20Hz. The sensitivity of atomic gravimetry is mainly limited by vibrational noise [39], which impacts the measurement sensitivity of atomic interferometry by affecting the stability of the Raman light phase. The transfer function of vibration noise can be expressed as Formula (13) [40]:

$$H_a(\omega) = \frac{4\sin\left(\frac{\omega T}{2}\right)^2}{(\omega T)^2} \tag{13}$$

where ω is the angular frequency of the vibration and T is the Raman pulse interval.

Taking T = 55 ms,we can calculate the effect of environmental vibration on the gravimeter as 71.162 μGal/$Hz^{1/2}$ and the effect of vibration on the gravimeter as 101.8327 μGal/$Hz^{1/2}$ during regular operation of the platform.

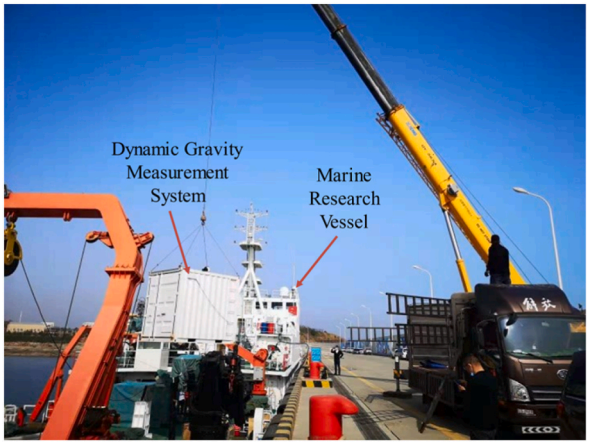

Fig. 11. The photo of hoisting dynamic absolute gravimetry system.

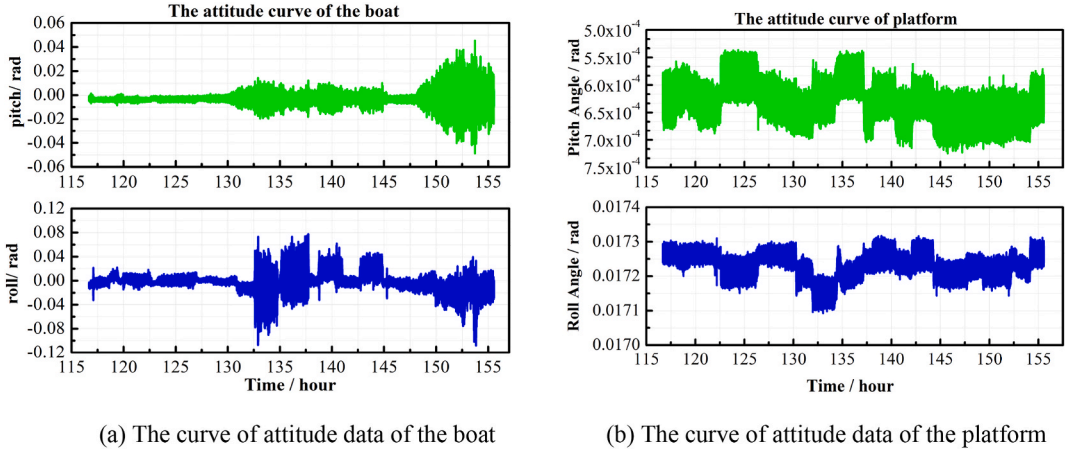

(a) The curve of attitude data of the boat (b) The curve of attitude data of the platform

Fig. 12. Comparison of attitude data from boat and platform.

Table 1
Statistical results of platform attitude data during navigation.

Platform attitude data	Roll angle/rad	Pitch angle/rad
Average	0.017	6.32×10^{-4}
Standard deviation	3.84×10^{-5}	3.32×10^{-5}

4.2. Shipboard experiment

Our group conducted absolute gravity measurement experiments at Zhoushan under ship mooring conditions [29], and the results showed that the platform was able to meet the requirements for static absolute gravity measurements on board. Subsequently, absolute gravity measurement experiments were carried out in the Yellow Sea for long-distance ocean voyages, as shown in Fig. 11.

We selected one of the navigation data of 36 h to compare the attitude of the hull with that of the ISP, and the comparison curves are shown in Fig. 12(a)(b). Fig. 12(a) shows the pitch and roll attitude data of the hull, and the maximum peak-to-peak value of the attitude angle of the hull reaches 0.2 rad.

The stability accuracy curve of the ISP is shown in Fig. 12(b) and the statistical results of mean and standard deviation are shown in Table 1. The standard deviation of both the pitch and roll is less than 4×10^{-5} rad, which meets the requirements of dynamic absolute gravity measurement for the angle of attitude. The reason for the non-zero mean value is the artificially set angle value to compensate for the installation error of the Raman light mirror.

The platform attitude curve in Fig. 12(b) shows a step caused by a solution error in the INS during the course change. The standard deviation of the platform attitude when the research vessel is travelling in a straight line meets the measurement requirements of the Cold Atomic Gravimeter.

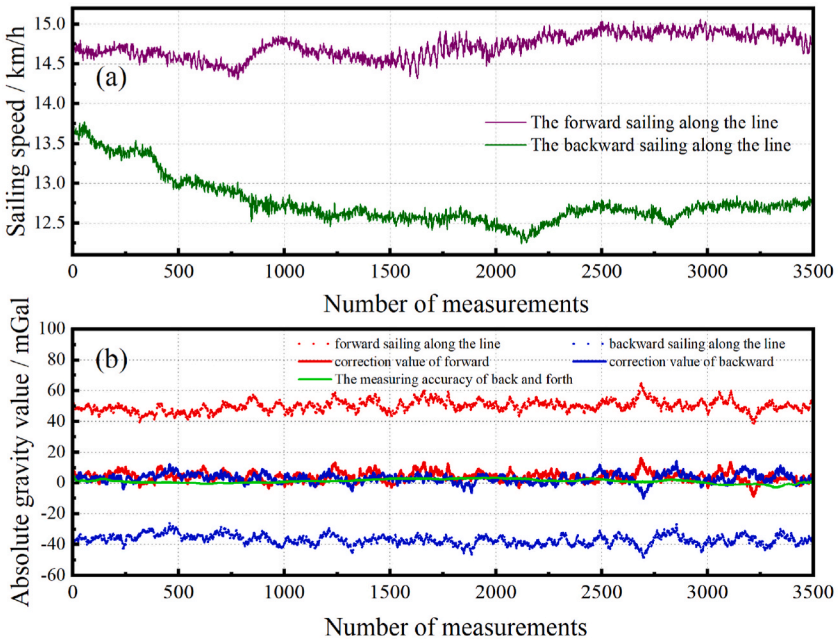

(a) The speed of the Vessel travels back and forth

(b) Gravity curves measured in straight lines and back

Fig. 13. The result of a straight round-trip measurement of gravity.

Then we select the absolute gravity measurement data obtained in one section of the straight round-trip route, subtract the absolute gravity value from the reference value 9.7934 m/s^2, as shown in red dots and blue dots point in Fig. 13(b), where the speed of ship on round-trip sailing is shown in Fig. 13(a), and the curve of the two sets of absolute gravity data after the corrected Coriolis effect is shown in red line and blue line in Fig. 13(b). After filtering, the gravity value curve measured on this line is shown in green line in Fig. 13(b), and its standard deviation is 1.4 mGal. The results show that ISP provides a high-precision horizontal attitude for dynamic absolute gravity measurement.

However, the current atomic gravimeter and inertially stabilized platform are too bulky and massive, making the process of transfer and assembly difficult. In the future, work will focus on developing a portable cold atomic gravimeter and a miniaturized inertially stabilized platform, reducing the size of the gravity probe, and combining the inertial navigation assembly with the gravity probe for attitude control, as shown in Figure (14).

5. Conclusion

Based on the measurement principle of cold atomic absolute gravimeter, this paper designs a high precision two-axis inertially stabilized platform for cold atomic absolute gravimeter and evaluates the stage vertical vibration noise. The effect of the vibration noise caused by the regular operation of the platform on the gravimetric measurement is 101.8327 μGal/Hz$^{1/2}$. Subsequently, a Yellow Sea navigation cruise test was conducted and the cruise attitude data showed that the platform had an attitude standard deviation of $\leq 4 \times 10^{-5}$ rad, and The standard deviation of the absolute gravity value of the linear round-trip measurement is 1.4 mGal, and the result achieves the expected goal of the dynamic measurement. The ISP is able to provide reliable attitude accuracy for dynamic absolute gravity measurements when the heading was held constant.

Data availability statement

The data that support the findings of this study are available from the corresponding author, Peng, upon reasonable request.

CRediT authorship contribution statement

Pei-jun Chen: Writing – review & editing, Writing – original draft, Visualization, Validation, Software, Methodology, Investigation, Formal analysis, Data curation, Conceptualization. **Min-rui Jiang:** Writing – review & editing, Writing – original draft, Software, Resources, Methodology, Investigation, Formal analysis, Data curation, Conceptualization. **Xiao-feng Lv:** Writing – review & editing,

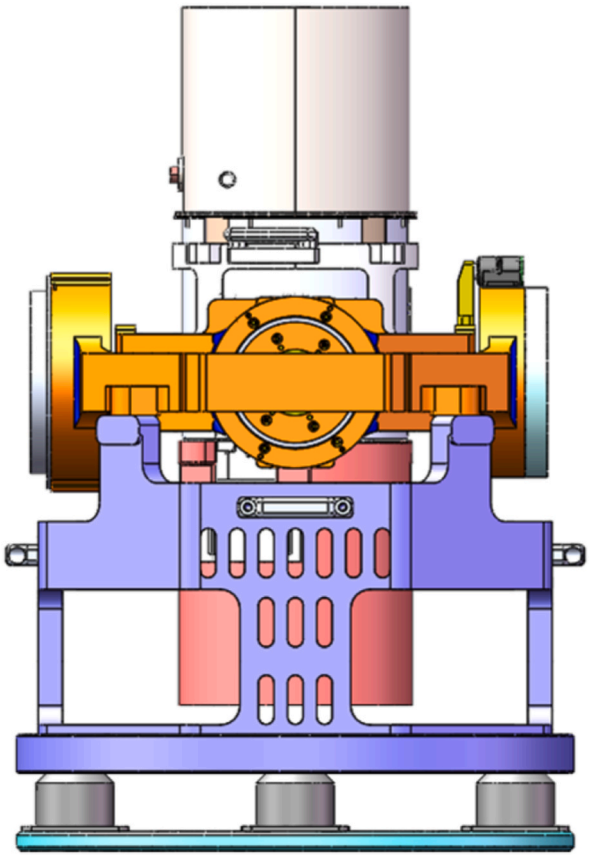

Fig. 14. Portable cold atomic absolute gravity measurement system.

Writing – original draft, Methodology. **Hang Zhou:** Methodology, Investigation. **Di Yang:** Investigation. **Ying Zhou:** Writing – review & editing, Resources, Project administration, Methodology. **Zifan Jin:** Investigation. **Shu-ping Peng:** Writing – review & editing, Writing – original draft, Visualization, Validation, Supervision, Software, Resources, Project administration, Methodology, Investigation, Funding acquisition, Formal analysis, Data curation, Conceptualization.

Declaration of competing interest

The authors declare the following financial interests/personal relationships which may be considered as potential competing interests:Shu-ping Peng reports financial support was provided by National Natural Science Foundation of China.

References

[1] Y. Sofyan, Y. Daud, J. Nishijima, Y. Fujimitsu, Y. Kamah, A. Yani, Y. Fukuda, M. Taniguchi, The first repeated absolute gravity measurement for geothermal monitoring in the Kamojang Geothermal Field, Indonesia, Geothermics 53 (2015) 114–124.
[2] Y. Fukuda, J.i. Okuno, K. Doi, C.-K. Lee, Gravity observations at Jang Bogo Station, Antarctica, and scale factor calibrations of different relative gravimeters, Polar Science 29 (2021), 100702.
[3] T. Niebauer, Gravimetric methods -absolute and relative gravity meter: instruments concepts and implementation, in: G. Schubert (Ed.), Treatise on Geophysics, second ed., Elsevier, Oxford, 2015, pp. 37–57.
[4] H. Yu, J. Guo, J. Li, D. Mu, Q. Kong, Zero drift and solid Earth tide extracted from relative gravimetric data with principal component analysis, Geodesy and Geodynamics 6 (2) (2015) 143–150.
[5] B. Fores, C. Champollion, N.L. Moigne, J. Chery, Impact of ambient temperature on spring-based relative gravimeter measurements, J. Geodesy 91 (3) (2017) 269–277.
[6] P. Křen, V. Pálinkáš, M. Vaľko, P. Mašika, Improved measurement model for FG5/X gravimeters, Measurement 171 (2021), 108739.
[7] M.J. Snadden, J.M. McGuirk, P. Bouyer, K.G. Haritos, M.A. Kasevich, Measurement of the Earth's gravity gradient with an atom interferometer-based gravity gradiometer, Phys. Rev. Lett. 81 (5) (1998) 971–974.
[8] D.W. Keith, C.R. Ekstrom, Q.A. Turchette, D.E. Pritchard, An interferometer for atoms, Phys. Rev. Lett. 66 (21) (1991) 2693–2696.
[9] J.P. Schwarz, D.S. Robertson, T.M. Niebauer, J.E. Faller, A free-fall determination of the Newtonian constant of gravity, Science 282 (5397) (1998) 2230–2234.
[10] S. Merlet, Q. Bodart, N. Malossi, A. Landragin, F.P.D. Santos, O. Gitlein, L. Timmen, Comparison between two mobile absolute gravimeters: optical versus atomic interferometers, Metrologia 47 (4) (2010) L9.
[11] K. Bongs, M. Holynski, J. Vovrosh, P. Bouyer, G. Condon, E. Rasel, C. Schubert, W.P. Schleich, A. Roura, Taking atom interferometric quantum sensors from the laboratory to real-world applications, Nature Reviews Physics 1 (12) (2019) 731–739.

[12] B. Fang, I. Dutta, P. Gillot, D. Savoie, J. Lautier, B. Cheng, C. Alzar, R. Geiger, S. Merlet, F. Pereira dos Santos, A. Landragin, Metrology with atom interferometry: inertial sensors from laboratory to field applications, J. Phys. Conf. (2016) 723.
[13] C.D. Panda, M. Tao, M. Ceja, A. Reynoso, H. Müller, Atomic gravimeter robust to environmental effects, Appl. Phys. Lett. 123 (6) (2023), 064001.
[14] B.S. Malek, Z. Pagel, X. Wu, H. Müller, Embedded control system for mobile atom interferometers, Rev. Sci. Instrum. 90 (7) (2019), 073103.
[15] A. Peters, K.Y. Chung, S. Chu, High-precision gravity measurements using atom interferometry, Metrologia 38 (1) (2001) 25.
[16] V. Menoret, P. Vermeulen, N. Le Moigne, S. Bonvalot, P. Bouyer, A. Landragin, B. Desruelle, Gravity measurements below 10^{-9} g with a transportable absolute quantum gravimeter, Sci. Rep. 8 (1) (2018), 12300.
[17] R. Reudink, R. Klees, O. Francis, J. Kusche, R. Schlesinger, A. Shabanloui, N. Sneeuw, L. Timmen, High tilt susceptibility of the Scintrex CG-5 relative gravimeters, J. Geodesy 88 (6) (2014) 617–622.
[18] K. Pyrchla, M. Pająk, J. Gołyga, J. Pyrchla, A model of the response of the MGS-6 gravity sensor to tilting, Measurement 188 (2022), 110573.
[19] B. Wu, B. Cheng, Z.-J. Fu, D. Zhu, Y. Zhou, K.-X. Weng, X.-L. Wang, Q. Lin, Measurement of absolute gravity based on cold atom gravimeter at large tilt angle, Acta Phys. Sin. 67 (19) (2018), 190302-190302.
[20] C. Glennie, K.P. Schwarz, A.M. Bruton, R. Forsberg, A.V. Olesen, K. Keller, A comparison of stable platform and strapdown airborne gravity, J. Geodesy 74 (2000) 383–389.
[21] S.K. Cai, J.B. Tie, K.D. Zhang, J.L. Cao, M.P. Wu, Marine gravimetry using the strapdown gravimeter SGA-WZ, MARINE GEOPHYSICAL RESEARCH 38 (4) (2017) 325–340.
[22] P. Wu, L. Liu, L. Wang, Y. Wang, M. Zhong, Z. Zhou, Z. Zou, A gyro-stabilized platform leveling loop for marine gravimeter, Rev. Sci. Instrum. 88 (2017), 064501.
[23] Y. Bidel, N. Zahzam, C. Blanchard, A. Bonnin, M. Cadoret, A. Bresson, D. Rouxel, M.F. Lequentrec-Lalancette, Absolute marine gravimetry with matter-wave interferometry, Nat. Commun. 9 (1) (2018) 627.
[24] Y. Bidel, N. Zahzam, A. Bresson, C. Blanchard, M. Cadoret, A. Olesen, R. Forsberg, Absolute airborne gravimetry with a cold atom sensor, J. Geodesy (2020) 94.
[25] Y. Bidel, N. Zahzam, A. Bresson, C. Blanchard, A. Bonnin, J. Bernard, M. Cadoret, T.E. Jensen, R. Forsberg, C. Salaun, S. Lucas, M.F. Lequentrec-Lalancette, D. Rouxel, G. Gabalda, L. Seoane, D.T. Vu, S. Bruinsma, S. Bonvalot, Airborne absolute gravimetry with a quantum sensor, comparison with classical technologies, J. Geophys. Res. Solid Earth 128 (4) (2023), e2022JB025921.
[26] H. Che, A. Li, J. Fang, G.-G. Ge, W. Gao, Y. Zhang, C. Liu, J.-N. Xu, L.-B. Chang, C.-F. Huang, W.-B. Gong, D.-Y. Li, X. Chen, F.-J. Qin, Ship-borne dynamic absolute gravity measurement based on cold atom gravimeter, Acta Phys. Sin. 71 (11) (2022).
[27] B. Wu, Y. Zhou, B. Cheng, D. Zhu, K.-N. Wang, X.-X. Zhu, P.-J. Chen, K.-X. Weng, Q.-H. Yang, J.-H. Lin, K.-J. Zhang, H.-L. Wang, Q. Lin, Static measurement of absolute gravity in truck based on atomic gravimeter, Acta Phys. Sin. 69 (6) (2020).
[28] B. Cheng, P.-J. Chen, Y. Zhou, K.-N. Wang, D. Zhu, L. Chu, K.-X. Weng, H.-L. Wang, S.-P. Peng, X.-L. Wang, B. Wu, Q. Lin, Experiment on dynamic absolute gravity measurement based on cold atom gravimeter, Acta Phys. Sin. 71 (2) (2022).
[29] B. Cheng, Y. Zhou, P.-J. Chen, K.-J. Zhang, D. Zhu, K.-N. Wang, K.-X. Weng, H.-L. Wang, S.-P. Peng, X.-L. Wang, B. Wu, Q. Lin, Absolute gravity measurement based on atomic gravimeter under mooring state of a ship, Acta Phys. Sin. 70 (4) (2021).
[30] Y. Zhou, C. Zhang, P.J. Chen, B. Cheng, D. Zhu, K.A. Wang, X.L. Wang, B. Wu, Z.K. Qiao, Q. Lin, R. Li, A testing method for shipborne atomic gravimeter based on the modulated Coriolis effect, SENSORS 23 (2) (2023).
[31] M.K. M, Inertially stabilized platforms for optical imaging systems, IEEE Control Syst. Mag. 28 (1) (2008) 47–64.
[32] J.M. H, Inertially stabilized platform technology Concepts and principles, IEEE Control Syst. Mag. 28 (1) (2008) 26–46.
[33] H.G. W, T.C. Williams, Strategic inertial navigation systems - high-accuracy inertially stabilized platforms for hostile environments, IEEE Control Syst. Mag. 28 (1) (2008) 65–85.
[34] T. Huynh, M.-T. Tran, D.-H. Lee, S. Chakir, Y.-B. Kim, A study on vision-based backstepping control for a target tracking system, Actuators 10 (5) (2021).
[35] J. Guo, C. Yuan, X. Zhang, F. Chen, Vision-based target detection and tracking for a miniature pan-tilt inertially stabilized platform, Electronics 10 (18) (2021).
[36] X. Zhou, B. Zhao, W. Liu, H. Yue, R. Yu, Y. Zhao, A compound scheme on parameters identification and adaptive compensation of nonlinear friction disturbance for the aerial inertially stabilized platform, ISA Trans. 67 (2017) 293–305.
[37] F. Dong, X. Lei, W. Chou, A dynamic model and control method for a two-Axis inertially stabilized platform, IEEE Trans. Ind. Electron. 64 (1) (2017) 432–439.
[38] J. Peterson, Observations and Modeling of Seismic Background Noise, u.s.geological survey open file report, 1993.
[39] J. Le Gouët, T.E. Mehlstäubler, J. Kim, S. Merlet, A. Clairon, A. Landragin, F. Pereira Dos Santos, Limits to the sensitivity of a low noise compact atomic gravimeter, Appl. Phys. B 92 (2) (2008) 133–144.
[40] G.M. Tino, G. Rosi, F. Sorrentino, L. Cacciapuoti, M. Prevedelli, Precision measurement of the gravitational constant with atom interferometry, in: 2013 Joint European Frequency and Time Forum & International Frequency Control Symposium, EFTF/IFC, 2013, pp. 593–598.